2D contact smooth formulation based on the mortar method

M. Tur[a] E. Giner[a] F.J. Fuenmayor[a] P. Wriggers[b]

[a]*Centro de Investigación de Tecnología de Vehículos, Universitat Politècnica de València, Camino de Vera s/n, 46022 Valencia, Spain*

[b]*Institut für Kontinuumsmechanik, Leibniz Universität Hannover, Appelstraße 11, 30167 Hannover, Germany*

Abstract

In this paper, we apply a smoothing technique to solve contact problems using a segment-to-segment formulation based on the mortar method. In contact smoothing the C^0 finite element description of the geometry is replaced by an improved smoothed one (usually with C^1 continuity). So far these techniques have been applied to solve contact problems based on node-to-segment interaction. Some numerical examples are solved to compare the performance of the smoothing and non-smoothing formulations. The examples show that the non-smoothed mortar formulation is improved mainly for problems with matching curved surfaces discretized with non-conforming meshes.

Key words: contact, mortar method, large sliding, Lagrange multiplier

1   Introduction

In recent years the mortar method has been successfully applied to solve large deformation contact problems [1–13] using both linear and quadratic elements in 2D or 3D. The aim of this work is to propose a mortar-based formulation to solve 2D large deformation frictionless contact problems using a smooth C^1 contact surface description of the two bodies. We consider linear elements in this work. The results will be compared with a non-smoothing formulation using linear elements also based on the mortar method [13] for some numerical problems.

A number of surface smoothing procedures have been proposed in the literature [14–19], in the context of node-to-segment (NTS) formulation. In contrast,

in this work the contact formulation is based on the mortar method so the contact constraints are imposed in a weak sense using integrals defined in the whole contact surface. Therefore, the proposed formulation has the advantages of segment-to-segment formulations, i.e. it avoids locking and overconstraining effects and it allows to obtain optimal convergence rates of the finite element solution.

In the node-to-segment smoothing formulations, a slave node interacts with a C^1 master surface. Different alternatives have been tried to define the C^1 smooth surface based on the nodal coordinates of the master nodes (nodes of the master surface): cubic Hermite interpolation [15,19], cubic Bernstein interpolation in the form of Bezier curve [18,14] or cubic splines [16]. In this work we choose a cubic Hermite interpolation. Since the proposed formulation is segment-to-segment, both the master surface and the slave surface are defined using the smooth interpolation. This is a significant difference with respect to node-to-segment formulations. In the clasical NTS formulation it is reported (see [14,15] for example) that the smoothing technique improves the quality of the solution and the robustness of contact algorithms, mainly for frictional problems. On the other hand, in the mortar method the room for improvement is less than in NTS because the mortar method already avoids some problems of NTS. This is due to the transmission of forces which is distributed in the whole contact surface and not only pointwise. However, there are some kind of problems solved with mortar formulation that can be improved, namely bodies with matching curved contact surfaces discretized with non-matching meshes. In this cases the error computing the gap can affect the global error of the finite element solution, as shown in the numerical examples. Another alternative to reduce the gap error could be the use of quadratic elements which are readily avaliable in the literature for the mortar formulation [5,7,9]

In this work the formulation and solution of the contact problem is performed following the same ideas exposed in [13]. We use the Lagrange multiplier method to impose the contact constraints and numerical integration is proposed to compute contact integrals. The linearization of the contact integrals is based on the value of the magnitudes at the quadrature points. The Newton-Raphson method is used to solve the non-linear problem.

The paper is organized as follows. Section 2 describes the formulation of the frictionless contact problem using Lagrange multipliers and the solution using finite elements. Section 3 details the definition of the smooth surfaces and how this definition is introduced in the evaluation of the segment-to-segment contact integrals. In Section 4 the linearization of the weak form is performed, in order to apply a Newton's method. In Section 5 several numerical examples are solved to compare the results of the smooth mortar contact formulation with that of mortar contact without smoothing, namely the implementation in [13]. Conclusions are exposed in Section 6. Appendix A shows details of the
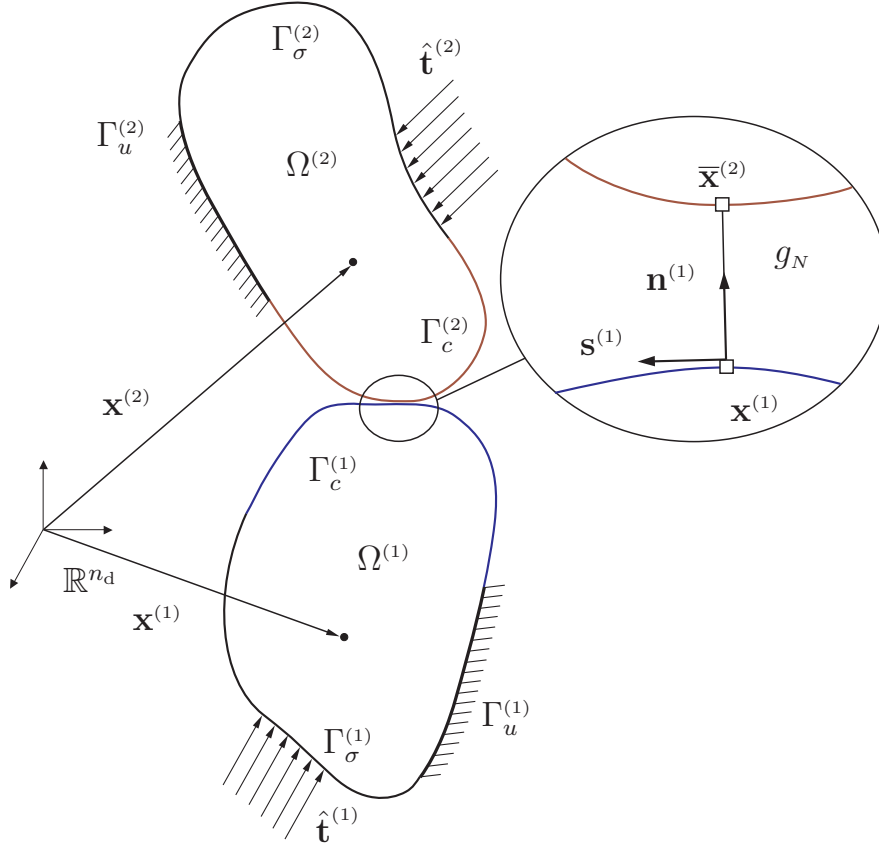
Fig. 1. Notation for the large deformation contact problem.

linearization and Appendix B the matrix notation.

2 Problem definition

2.1 Contact problem formulation

In figure 1 there is a schematic of two 2D bodies $\Omega^{(i)}$ in contact represented in the deformed configuration. $\Gamma_u^{(i)}$ and $\Gamma_\sigma^{(i)}$ are the boundaries with prescribed displacements and tractions, respectively. The portion of the boundary where the body can be in contact is denoted by $\Gamma_c^{(i)}$. The contact surfaces $\Gamma_c^{(1)}$ and $\Gamma_c^{(2)}$ are denoted as slave and master surfaces, respectively.

For every point in the slave surface $\mathbf{x}^{(1)}$, the contact point on the master surface $\overline{\mathbf{x}}^{(2)}$ is computed as the intersection of the surface $\Gamma_c^{(2)}$ with the line having direction of the normal vector $\mathbf{n}^{(1)}$, as depicted in figure 1. $\mathbf{n}^{(1)}$ is the unit normal vector to the slave surface. The normal gap at a given point $\mathbf{x}^{(1)}$

3

of the slave surface is defined as

$$g_N = \left(\overline{\mathbf{x}}^{(2)} - \mathbf{x}^{(1)}\right) \cdot \mathbf{n}^{(1)} \tag{1}$$

where the convective coordinate on surface 2, $\xi^{(2)}$ is used to define the contact point as $\overline{\mathbf{x}}^{(2)} = \mathbf{x}^{(2)}(\overline{\xi}^{(2)})$.

The virtual work principle can be written as the sum of the virtual work of internal and external forces of the two bodies and the virtual work of contact forces

$$G(\mathbf{v}, \mathbf{u}) = \sum_{i=1}^{2} \left(G_{int}^{(i)}(\mathbf{v}, \mathbf{u}) + G_{ext}^{(i)}(\mathbf{v}) \right) + G_C(\mathbf{v}) = 0 \tag{2}$$

where $\mathbf{u}$ are the displacements and $\mathbf{v}$ their variations. The virtual work arising from the internal and external forces can be computed for body (i) in the deformed configuration as

$$G_{int}^{(i)}(\mathbf{v}, \mathbf{u}) + G_{ext}^{(i)}(\mathbf{v}) = \int_{\Omega^{(i)}} \boldsymbol{\sigma} \cdot \operatorname{grad} \mathbf{v} \, d\Omega - \int_{\Omega^{(i)}} \mathbf{b} \cdot \mathbf{v} \, d\Omega - \int_{\Gamma_\sigma^{(i)}} \hat{\mathbf{t}} \cdot \mathbf{v} \, d\Gamma \tag{3}$$

where $\boldsymbol{\sigma}$ is the Cauchy stress tensor, $\mathbf{b}$ denotes the body forces and $\hat{\mathbf{t}}$ the prescribed tractions.

The contact virtual work is also computed in the current configuration. Taking the slave surface $\Gamma_c^{(1)}$ as integration domain and taking into account that the Cauchy contact traction has opposite direction in each body $\mathbf{t}_C^{(2)} = -\mathbf{t}_C^{(1)}$ and the slave and master surfaces are equal in the real contact area Γ_c, the contact virtual work can be written as

$$\begin{aligned} G_c(\mathbf{v}) &= \int_{\Gamma_c^{(1)}} \mathbf{t}_C^{(1)} \cdot \mathbf{v}^{(1)} \, d\Gamma + \int_{\Gamma_c^{(2)}} \mathbf{t}_C^{(2)} \cdot \mathbf{v}^{(2)}(\overline{\xi}^{(2)}) \, d\Gamma \\ &= -\int_{\Gamma_c} \mathbf{t}_C^{(1)} \cdot \left(\mathbf{v}^{(2)}(\overline{\xi}^{(2)}) - \mathbf{v}^{(1)} \right) \, d\Gamma \end{aligned} \tag{4}$$

The variation of the gap δg_N obtained from equation 1 is

$$\delta g_N = \left(\mathbf{v}^{(2)}(\overline{\xi}^{(2)}) - \mathbf{v}^{(1)} \right) \cdot \mathbf{n}^{(1)} \tag{5}$$

and the contact pressure p_N can be defined as the normal component of the contact traction as $p_N = -\mathbf{t}_C^{(1)} \cdot \mathbf{n}^{(1)}$. Taking into account this definition and equation 5, the contact virtual work of equation 4 can be rewritten as

$$G_c(\mathbf{v}) = \int_{\Gamma_c} p_N \, \delta g_N \, d\Gamma \tag{6}$$

Note that in the real contact area we consider that the distance between the bodies in the continuum, i.e. the gap, is zero and the surfaces of both bodies are parallel.

4

The size and position of the contact interface is computed to verify the Kuhn-Tucker conditions

$$g_N \geq 0, \qquad p_N \geq 0, \qquad p_N \, g_N = 0 \tag{7}$$

2.2 Solution by the finite element method

In this work the bodies are discretized using two dimensional bilinear finite elements. In each body the displacement field, its variation and the current coordinates are interpolated as follows

$$\mathbf{v}^{(i)h} = \sum_{k=1}^{n_n} N_k^{(i)}(\xi) \, \mathbf{v}_k^{(i)} \quad , \qquad \mathbf{x}^{(i)h} = \sum_{k=1}^{n_n} N_k^{(i)}(\xi) \, \mathbf{x}_k^{(i)} \tag{8}$$

where $N_k^{(i)}$ is the shape function of node k in body (i), n_n is the number of nodal points and $\mathbf{x}_k^{(i)}$ and $\mathbf{v}_k^{(i)}$ are the nodal values of $\mathbf{x}^{(i)}$ and $\mathbf{v}^{(i)}$, respectively. With these definitions the virtual work terms of internal and external forces of equation 3 can be evaluated using the standard finite element formulation and the equivalent nodal force can be obtained

$$\sum_{i=1}^{2} \left(G_{int}^{h,(i)}(\mathbf{v}, \mathbf{u}) + G_{ext}^{h,(i)}(\mathbf{v}) \right) = \mathbf{v} \cdot \left(\mathbf{f}^{i} + \mathbf{f}^{e} \right) \tag{9}$$

For the computation of the contact virtual work, the nodes of the slave surface are divided into two sets: the active set for nodes in contact and the inactive set for nodes out of the contact. Only the active nodes contribute to the finite element formulation with a nodal force due to the contact virtual work and a constraint equation.

The contact virtual work in the discretized domain is obtained following an approach similar to that presented in [4] and [13] which is based on the Lagrange multiplier method. An additional variable, the Lagrange multiplier λ_N is introduced which has units of contact pressure. In the above references the virtual work of the contact forces is derived from the variation of the contact potential energy with respect to displacements, and a expression similar to equation 6 is obtained. In the discretized domain this integral is evaluated along the slave surface $\Gamma_c^{(1)h}$. This surface is divided into segments $\Gamma_{c_{ks}}^{(1)}$ and the integral is computed as the contribution of all segments. A mapping between the current configuration of the segment and the reference element (with coordinate $\xi \in [-1, 1]$) is defined and the contact virtual work can be written as

$$G_C^h(\mathbf{v}^h) = \sum_{\forall c_{ks}} \left(\int_\square \lambda_N^h \, \delta g_N^h \, J \, d\xi + \int_\square \lambda_N^h \, g_N^h \, \delta J \, d\xi \right) = \mathbf{v} \cdot \mathbf{f}_N^c \tag{10}$$

where J is the jacobian of the mapping (in case of 2D linear elements is the length of the deformed slave segment divided by 2). The square symbol in the

integrals is used to denote the integration is performed in the reference element. As pointed out in [4,13] the second integral of equation 10 is always zero due to the Kuhn-Tucker conditions, but it is necessary to obtain a symmetric tangent matrix in the linearization. The variation of the gap is based on the smoothed surface definitions and it is detailed in the next section.

The interpolation of the Lagrange multiplier field is based on linear shape functions. Given a nodal value of the Lagrange multiplier λ_{Nk}, the interpolation of the multipliers and their variations are defined as

$$\lambda_N^h = \sum_{k=1}^{n_c} M_k^{(1)}(\xi)\, \lambda_{Nk} \qquad\qquad \delta\lambda_N^h = \sum_{k=1}^{n_c} M_k^{(1)}(\xi)\, \delta\lambda_{Nk} \qquad (11)$$

where n_c is the number of active nodes in the slave surface $\Gamma_c^{(1)}$.

Like in all mortar-based contact formulations, we define an averaged gap $\widehat{g}_{Nk}$ using the Lagrange multiplier shape functions for every slave node k.

$$\widehat{g}_{Nk} = \int_{\Gamma_c^{(1)h}} M_k\, g_N^h\, d\Gamma = \int_{\square} M_k\, g_N^h\, J\, d\xi \qquad (12)$$

The finite element formulation of the contact problem consists in finding the displacement and Lagrange fields that fulfill the following equations

$$\begin{aligned} \mathbf{f}^{\text{i}} + \mathbf{f}^{\text{e}} + \mathbf{f}_N^{\text{c}} &= 0 \\ \widehat{\mathbf{g}}_N &= 0 \end{aligned} \qquad (13)$$

Note that the contribution to the contact force and the contact constraint is only due to the active nodes. An algorithm is defined to find the correct active set (see [13] for more details on the algorithm).

3   Discretization using smooth surfaces

The evaluation of the contact integrals (equations 10 and 12) needs the definition of the gap and its variation based on the smoothing surface formulation. In this work, cubic Hermite polynomials are used to define the master and slave surfaces. In figure 2 there is a slave segment c_{ks} with slave nodes $ks-1$ and ks. The deformed configuration of the smoothed surface is based on the position of the nodes $\mathbf{x}^{ks-1}$ and $\mathbf{x}^{ks}$ and the averaged tangent vectors $\hat{\mathbf{s}}^{ks-1}$ and

$\hat{\mathbf{s}}^{ks}$ and is defined as follows:

$$\mathbf{xs}^{(1)}(\xi) = He_1(\xi)\,\mathbf{x}^{ks-1} + He_2(\xi)\,\mathbf{x}^{ks} + He_3(\xi)\,\hat{\mathbf{s}}^{ks-1} + He_4(\xi)\,\hat{\mathbf{s}}^{ks}$$

$$
\begin{aligned}
He_1(\xi) &= \frac{(\xi-1)^2\,(2+\xi)}{4} \\
He_2(\xi) &= \frac{(\xi+1)^2\,(2-\xi)}{4} \\
He_3(\xi) &= \frac{(\xi-1)^2\,(\xi+1)}{4} \\
He_4(\xi) &= \frac{(\xi+1)^2\,(\xi-1)}{4}
\end{aligned}
\tag{14}
$$

The averaged tangent vectors, as well as the averaged normal vectors, are not unitary and are calculated form the finite element discretization as

$$\hat{\mathbf{s}}^{ks} = \frac{\dfrac{\mathbf{x}^{ks+1}-\mathbf{x}^{ks}}{2} + \dfrac{\mathbf{x}^{ks}-\mathbf{x}^{ks-1}}{2}}{2} = \frac{\mathbf{x}^{ks+1}-\mathbf{x}^{ks-1}}{4} \tag{15}$$
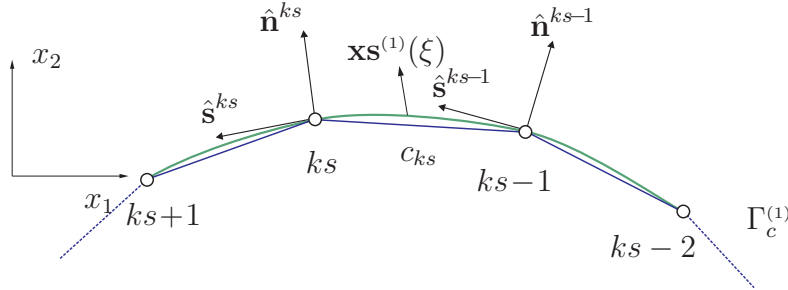

Fig. 2. Smoothed slave surface using Hermite polynomials.

Substituting equation 15 in the definition of the smoothed slave surface (equation 14) we obtain

$$\mathbf{xs}^{(1)}(\xi) = H_1(\xi)\,\mathbf{x}^{ks-2} + H_2(\xi)\,\mathbf{x}^{ks-1} + H_3(\xi)\,\mathbf{x}^{ks} + H_4(\xi)\,\mathbf{x}^{ks+1}$$

with

$$
\begin{aligned}
H_1(\xi) &= -\frac{He_3}{4} \\
H_2(\xi) &= He_1 - \frac{He_4}{4} \\
H_3(\xi) &= He_2 + \frac{He_3}{4} \\
H_4(\xi) &= \frac{He_4}{4}
\end{aligned}
\tag{16}
$$

where it can be observed the dependence of the slave surface on the position of four consecutive nodes associated to each slave segment.

7

The master surface is defined similarly. In order to compute the contact integrals we need to define the gap and its variation. This is shown schematically in figure 3. For a given quadrature point in the smoothed slave surface $\xi_g^{(1)}$, the gap is computed in three steps:

- 1. Compute the global position of the slave surface at the quadrature point $\xi_g^{(1)}$ using the Hermite surface description of equation 16.

- 2. Obtain the unit vector normal to the slave surface as $\mathbf{n}^{(1)}{}_g = \dfrac{\hat{\mathbf{n}}_g^{(1)}}{\|\hat{\mathbf{n}}_g\|}$, where $\hat{\mathbf{n}}_g = \hat{\mathbf{s}}_g \times \mathbf{e}_3$ and the tangent vector is computed from equation 16 as

$$\mathbf{s}^{\hat{(1)}}{}_g = \frac{\partial \mathbf{xs}^{(1)}(\xi_g^{(1)})}{\partial \xi} \tag{17}$$

- 3. Solve the intersection between the line having the normal direction and the cubic Hermite polynomial for the master surface (cubic equation).

$$\mathbf{x}_g + g_{Ng}\,\mathbf{n}_g(\xi_g^{(1)}) = \mathbf{xs}^{(2)}(\xi_g^{(2)}) \tag{18}$$

where master surface is defined using a smooth interpolation like the slave surface

$$\begin{aligned}\mathbf{xs}^{(2)}(\xi_g^{(2)}) = \\ H_1(\xi_g^{(2)})\,\mathbf{x}^{km-2} + H_2(\xi_g^{(2)})\,\mathbf{x}^{km-1} + H_3(\xi_g^{(2)})\,\mathbf{x}^{km} + H_4(\xi_g^{(2)})\,\mathbf{x}^{km+1}\end{aligned} \tag{19}$$

Solving equation 18, we obtain the gap g_N^g and the local coordinate $\bar{\xi}_g^{(2)}$ of the contact point in the master surface.
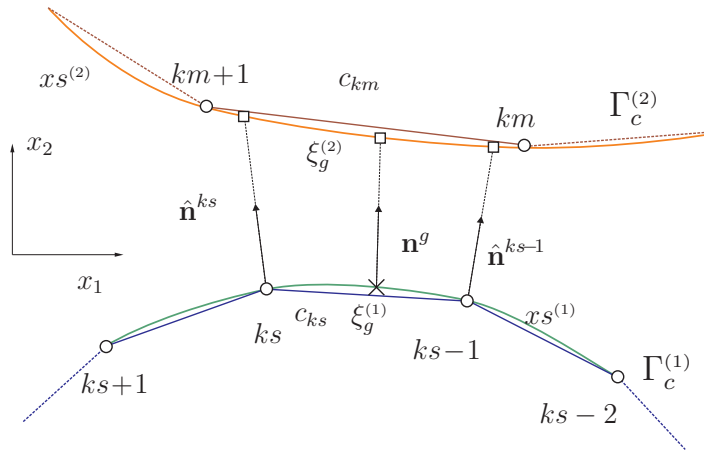

Fig. 3. Interaction between the two smoothed surfaces.

Taking variations of equation 18 the following expression is obtained

$$\mathbf{v}_g^{(1)} + \delta g_{Ng}\,\mathbf{n}_g^{(1)} + g_{Ng}\,\delta\mathbf{n}^{(1)} = \mathbf{v}^{(2)}(\xi_g^{(2)}) + \hat{\mathbf{s}}_g^{(2)}\,\delta\xi_g^{(2)} \tag{20}$$

8

The variation of the master surface $\delta\mathbf{xs}^{(2)}(\xi_g^{(2)})$ is divided into two terms. The first one, $\mathbf{v}^{(2)}$, is computed like in equation 19 but replacing the position of the nodes by the variation of displacements. The second one is obtained taking the variation with respect to the local coordinate of the contact point as

$$\mathbf{xs}_{,\xi}^{(2)}\,\delta\xi = \left(H_{1,\xi}\,\mathbf{x}^{km-2} + H_{2,\xi}\,\mathbf{x}^{km-1} + H_{3,\xi}\,\mathbf{x}^{km} + H_{4,\xi}\,\mathbf{x}^{km+1}\right)\delta\xi \qquad (21)$$

The virtual gap is computed by multiplying equation 20 by the unit normal vector $\mathbf{n}_g^{(1)}$

$$\delta g_{Ng} = \left(\mathbf{v}^{(2)}(\xi_g^{(2)}) - \mathbf{v}_g^{(1)}\right)\cdot\mathbf{n}_g^{(1)} + \hat{\mathbf{s}}^{(2)}\cdot\mathbf{n}_g^{(1)}\,\delta\xi_g^{(2)} \qquad (22)$$

Note the the second term in the right hand side of the last equation is, in general, nonzero because vectors $\hat{\mathbf{s}}_g^{(2)}$ and $\mathbf{n}_g^{(1)}$ are not necessarily perpendicular. The variable $\delta\xi_g^{(2)}$ is obtained by multiplying equation 20 by the unit tangent vector $\mathbf{s}_g^{(1)}$ (which is perpendicular to $\mathbf{n}_g^{(1)}$) and simplifying

$$\delta\xi_g^{(2)} = \frac{-\left(\mathbf{v}^{(2)}(\xi_g^{(2)}) - \mathbf{v}_g^{(1)}\right)\cdot\mathbf{s}_g^{(1)} + g_{Ng}\,\delta\mathbf{n}_g^{(1)}\cdot\mathbf{s}_g^{(1)}}{\hat{\mathbf{s}}_g^{(2)}\cdot\mathbf{s}_g^{(1)}} \qquad (23)$$

3.1   Contribution of the active nodes. Numerical integration

There are two alternatives to perform the numerical integration of the contact integrals. The first one, is to perform a segmentation of the slave segment in subsegments where the integrand is a unique polynomial. For example in the segment of figure 4 there are two subsegments. A quadrature rule is employed in each subsegment to perform the integration. Using this strategy the numerical integration error is eliminated, but the computational cost is increased.

The second option, which is used in this work and in the numerical examples of section 5, is to define a set of quadrature points in each slave segment, without taking into account how the variation of the integrand function is (see figure 4). In the case of the example shown in figure 4, more than one master segment interact with a slave segment, and therefore there is an error in the numerical evaluation of the contact integral. This error can be reduced by increasing the number of quadrature points. This integration was also used in a non-smooth mortar based formulation [13].

Using the numerical quadrature with N_g points in each segment the contact virtual work is computed as

$$G_N^h(\mathbf{v}^h) = \sum_{\forall c_{ks}}\sum_{g=1}^{N_g} H_g\,\lambda_{Ng}\,\delta g_{Ng}\,J_g \qquad (24)$$

where H_g is the weight of the quadrature point and J_g is the jacobian at the quadrature point. The Lagrange multiplier at the quadrature point λ_{Ng} is
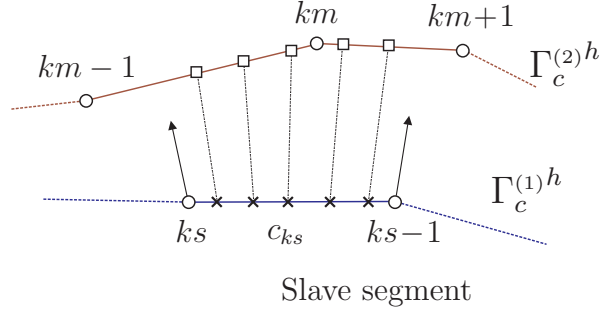
9

Fig. 4. Slave segment and numerical integration.

computed using equation 11 and depends on the nodal values of the multiplier. The virtual gap δg_{N_g} is obtained from equation 22.

The calculus of jacobian and the matrix expression of the virtual gap is detailed in the appendix.

4 Linearization

A semi-smooth Newton method is used to solve the non-linear equations 13 derived from the discretization of of contact problem. The contact contribution is due to the active nodes in two terms: the contact virtual work (equation 10) and the constraint (equation 13). Linearizing each term of these equations we obtain

$$\Delta G_N^h = \int_\square \Delta\lambda_N^h\, \delta g_N^h\, J\, d\xi + \int_\square \lambda_N^h\, \Delta\delta g_N^h\, J\, d\xi + \int_\square \lambda_N^h\, \delta g_N^h\, \Delta J\, d\xi$$
$$+ \int_\square \Delta\lambda_N^h\, g_N^h\, \delta J\, d\xi + \int_\square \lambda_N^h\, \Delta g_N^h\, \delta J\, d\xi + \int_\square \lambda_N^h\, g_N^h\, \Delta\delta J\, d\xi \qquad (25)$$
$$\Delta\widehat{\mathbf{g}_N} = \int_\square \delta\lambda_N^h\, \Delta g_N^h\, J\, d\xi + \int_\square \delta\lambda_N^h\, g_N^h\, \Delta J\, d\xi$$

The same numerical integration defined in section 3.1 can be used to compute the integrals of equation 25. Therefore the integrands have to be evaluated at the quadrature points. Due to the equivalence between variations and linearizations, equations 22 and 23 can be rewritten replacing $\Delta(\dots)$ by $\delta(\dots)$ so that the linearization of the gap Δg_N^h can be obtained directly from equation 22. Since the multiplier λ_N is a free variable $\Delta\lambda_N$ is directly its linearization. The variation and linearization of the jacobian and normal vectors is detailed in the Appendix.

10

The linearization of the virtual gap can be obtained linearizing equation 20

$$\Delta\delta g_{Ng}\, \mathbf{n}_g^{(1)} + \delta g_{Ng}\, \Delta\mathbf{n}_g^{(1)} + \Delta g_{Ng}\, \delta\mathbf{n}_g^{(1)} + g_{Ng}\, \Delta\delta\mathbf{n}_g^{(1)} =$$
$$\delta\hat{\mathbf{s}}^{(2)}\, \Delta\bar{\xi}_g^{(2)} + \Delta\hat{\mathbf{s}}_g^{(2)}\, \delta\bar{\xi}_g^{(2)} + \hat{\mathbf{s}}_g^{(2)}\, \Delta\delta\bar{\xi}_g^{(2)} \tag{26}$$

Multiplying by the unit normal vector and simplifying we obtain

$$\Delta\delta g_{Ng} = \delta\hat{\mathbf{s}}^{(2)} \cdot \mathbf{n}_g^{(1)}\, \Delta\xi_g^{(2)} + \Delta\hat{\mathbf{s}}^{(2)} \cdot \mathbf{n}_g^{(1)}\, \delta\xi_g^{(2)}$$
$$+ \hat{\mathbf{s}}^{(2)} \cdot \mathbf{n}_g^{(1)}\, \Delta\delta\xi_g^{(2)} - g_{Ng}\, \mathbf{n}_g^{(1)} \cdot \Delta\delta\mathbf{n}_g^{(1)} \tag{27}$$

The term $\Delta\delta\xi_g^{(2)}$ is obtained by multiplying equation 26 by the unit tangent vector $\mathbf{s}_g^{(1)}$

$$\hat{\mathbf{s}}_g^{(2)} \cdot \mathbf{s}_g^{(1)}\, \Delta\delta\xi_g^{(2)} = -\delta\hat{\mathbf{s}}_g^{(2)} \cdot \mathbf{s}_g^{(1)}\, \Delta\xi_g^{(2)} - \Delta\hat{\mathbf{s}}_g^{(2)} \cdot \mathbf{s}_g^{(1)}\, \delta\xi_g^{(2)}$$
$$\delta g_{Ng}\, \Delta\mathbf{n}_g^{(1)} \cdot \mathbf{s}_g^{(1)} + \Delta g_{Ng}\, \delta\mathbf{n}_g^{(1)} \cdot \mathbf{s}_g^{(1)} + g_{Ng}\, \Delta\delta\mathbf{n}_g^{(1)} \cdot \mathbf{s}_g^{(1)} \tag{28}$$

Within the above definitions the numerical integration of the contact force, gap vector and its linearizations can be performed. The system of equations to be solved during each Newton iteration has the following form

$$\begin{bmatrix} \mathbf{K}_G + \mathbf{K}_N & \mathbf{C}_N^T \\ \mathbf{C}_N & 0 \end{bmatrix} \begin{pmatrix} \Delta\mathbf{u} \\ \Delta\lambda_N \end{pmatrix} = - \begin{pmatrix} \mathbf{f}^{\mathrm{i}} + \mathbf{f}^{\mathrm{e}} + \mathbf{f}_N^{\mathrm{c}} \\ \mathbf{g}_N \end{pmatrix} \tag{29}$$

where $\mathbf{K}_G$ comes from the linearization of internal and external forces and $\mathbf{K}_N$ and $\mathbf{C}_N$ are detailed in matrix form in the Appendix.

5 Numerical examples

Some numerical examples have been solved to test the performance of the proposed smoothing formulation. The results are compared with the non-smoothed mortar implementation presented in [13] which is based on linear elements. As was done in [13], the displayed contact pressure is obtained with a linear interpolation from the nodal values that are computed as the equivalent nodal force divided by the equivalent nodal area:

$$p_{Nk} = -\frac{\int_{\Gamma_c^{(1)h}} N_k\, \lambda_N^h\, d\Gamma}{\int_{\Gamma_c^{(1)h}} N_k\, d\Gamma} \tag{30}$$

where N_k is the shape function associated to slave node k.

Examples 5.1 and 5.3 are small deformation and large deformation problems, respectively, with matching curved surfaces in contact that are discretized with non-matching meshes. This is the kind of problems in which the smoothed formulation is expected to improve the most compared with non-smoothed formulation using linear elements. Although the examples involve academic problems, they show clearly the interactions that arise between meshes under this configuration. That could appear in certain problems in practice. It is worth pointing out that a non-smoothed mortar formulation using quadratic elements could be an alternative to the smoothing technique in order to reduce the gap error in curved surfaces.

Example 5.2 is a well known problem solved by other authors [3,9] to test the convergence of the semi-smooth Newton method. Finally, example 5.4 is presented to point out that the smoothing method does not always improve results and other techniques like the adaptive mesh refinement can be used instead.

In all the examples the number of quadrature points in every slave segment is $N_g = 16$. This number has been chosen to ensure that, in practice, a larger number of quadrature points does not modify the finite element solution in the four examples.

5.1   *Cylinder under internal pressure*

The first problem is a hollow cylinder subject to internal pressure under small deformation conditions and linear elastic material behavior. The schematic of the problem is shown in figure 5.1 where it can be seen that only a quarter of the hollow cylinder is considered and the cylinder is divided into two bodies in contact. The dimensions of the cylinder are $a = 0.9$, $b = 1.1$ and $c = 1.0$. The Young's modulus is $E = 100$ and the Poisson's ratio is $\upsilon = 0.3$. This problem has an exact solution and therefore, the exact error of the finite element solution can be computed.

The problem was solved using meshes with different slave to master element size ratios 1:4, 1:2, 3:4, 9:10 (see figure 6) and a 1:1 conforming mesh (not shown in the figure). In this figure, the meshes of the two bodies in contact are shifted to clarify the representation since both clearly overlap. We have used the discretized surfaces to compute the initial gap, although this is a small deformation problem and it could be solved taking into account that the theoretical value of the initial gap is zero. This is done to analyze the effect of the initial gap error for non-matching meshes.

Every mesh in figure 6 is the first of a sequence of meshes obtained by uniform refinement. These meshes are used to analyze the error of the finite element
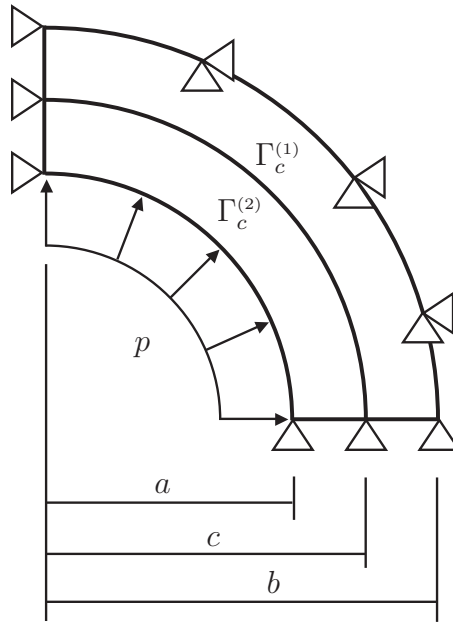
Fig. 5. Schematic of the cylinder under internal pressure problem.

solution. Note that the ratio between master and slave element size is kept constant during the refinement. The exact error in energy and L_2 norms are plotted in figure 7 as a function of the number of degrees of freedom of the mesh. A comparison is performed for every mesh using non-smoothed (dotted line) and smoothed formulations (continuous line). The $\circ$ symbol is used for the 1:4 meshes, $\square$ symbol for the 1:2 meshes, $\triangle$ for the 3:4 meshes, $\times$ symbol for the 9:10 meshes and $+$ symbol for the conforming 1:1 mesh. In the last case only the smoothed formulation results are plotted.

In this problem there are two sources of error: the discretization error and the error due to the initial gap. As can be seen in figure 7, the higher the ratio between master and slave element size, the higher error of the solution is. Of course, the 1:4 mesh is very poorly suited if the error due to initial gap is to be minimized, so the global error in the solution expected for the first meshes is very high. At the other end, in the 1:1 mesh the initial gap is zero because the meshes are conforming by construction and we have only the discretization error. The error of the first 1:4 mesh is high compared with the 1:1 for both smoothed and non-smoothed formulations, although in the smoothed case the error is one order of magnitude lower.

It can be remarked that the convergence in the energy norm asymptotically tends to the same value for every mesh using the two formulations. However the convergence in L_2 norm exhibits a constant gap. This is due to the influence of the geometrically computed initial gap in the global error of the solution and its convergence. The discretization error converges with the element size h as $O(h^1)$ in energy norm and $O(h^2)$ in L_2 norm ($O(n_{dof}^{0.5})$ and $O(n_{dof}^1)$, respectively in 2D problems). On the other hand, the convergence of the error
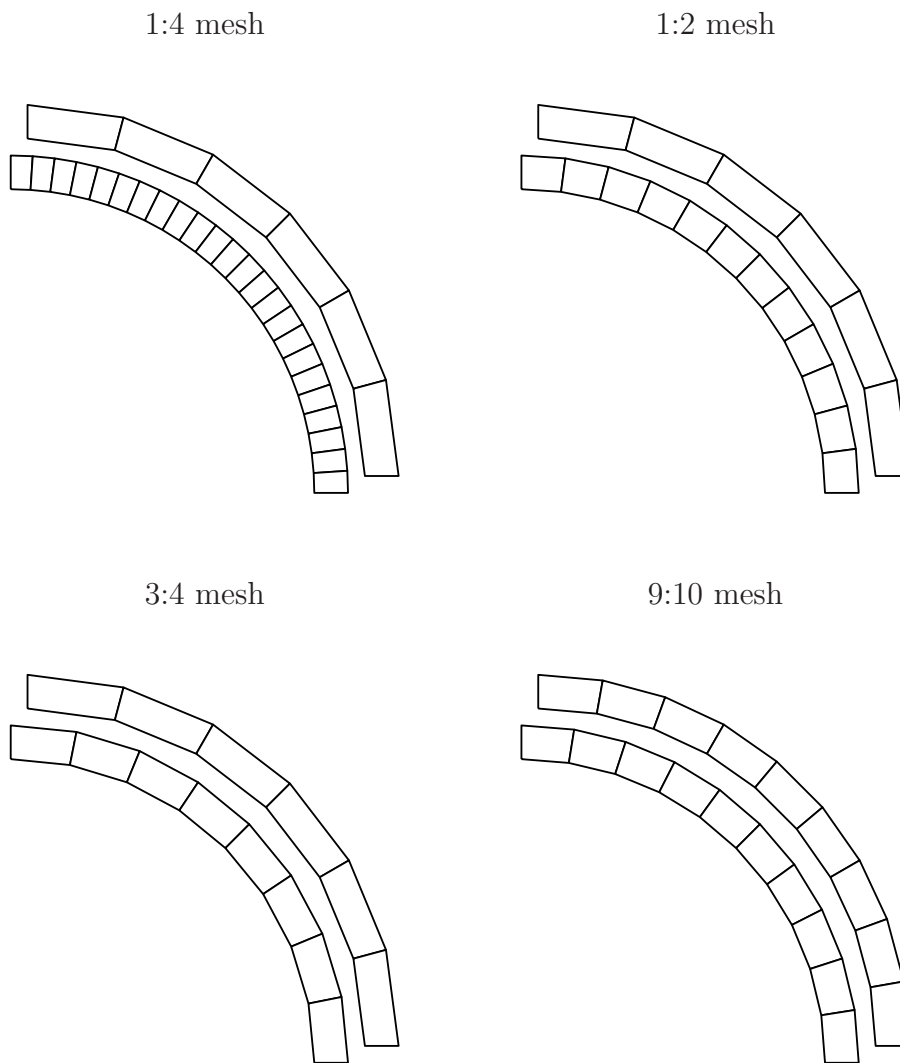
13

Fig. 6. Meshes used to solve the cylinder problem.

due to the initial gap depends on the formulation. In this problem, for very different sizes of slave and master elements, the geometrical error in the initial gap decreases as $O(h^2)$ for the non smoothed formulation. This means that its contribution to the global error decreases as $O(h^2)$ (that is $O(n_{dof}^1)$) in both L_2 and energy norms. In the smoothed formulation the error due to initial gap decreases faster in both norms.

As a conclusion of the above discussion we find that the global error in energy norm tends to the same value for smoothed and non-smoothed formulations because the error due to the initial gap converges faster than the discretization error. Therefore, as the number of degrees of freedom increases the discretization error becomes dominant. In the case of L_2 norm the error due to initial gap converges faster than the discretization error for the smoothed formula-
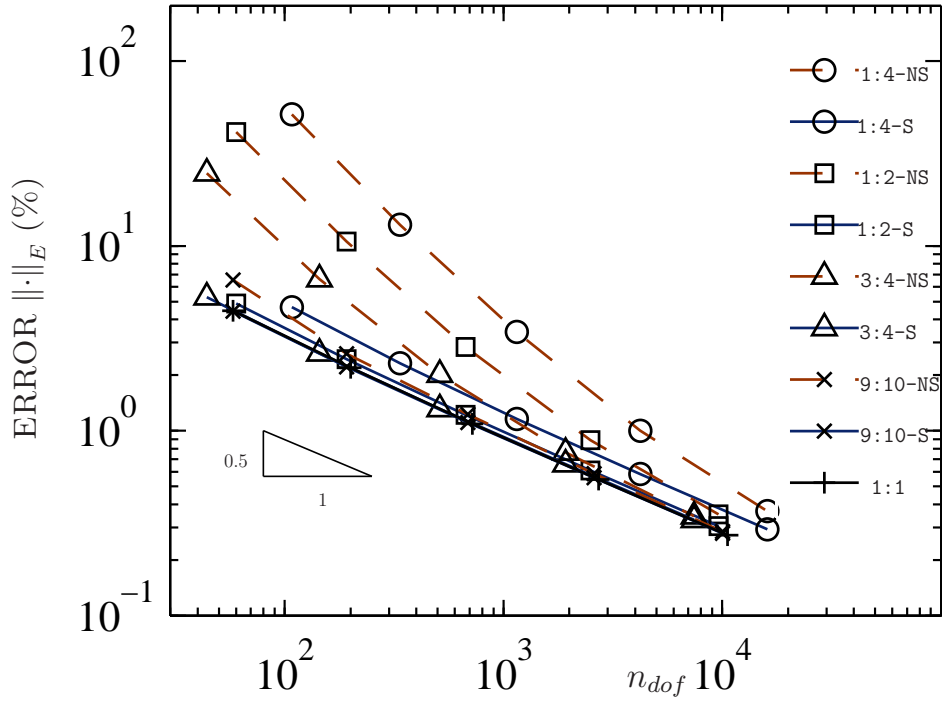
(a) Error in energy norm
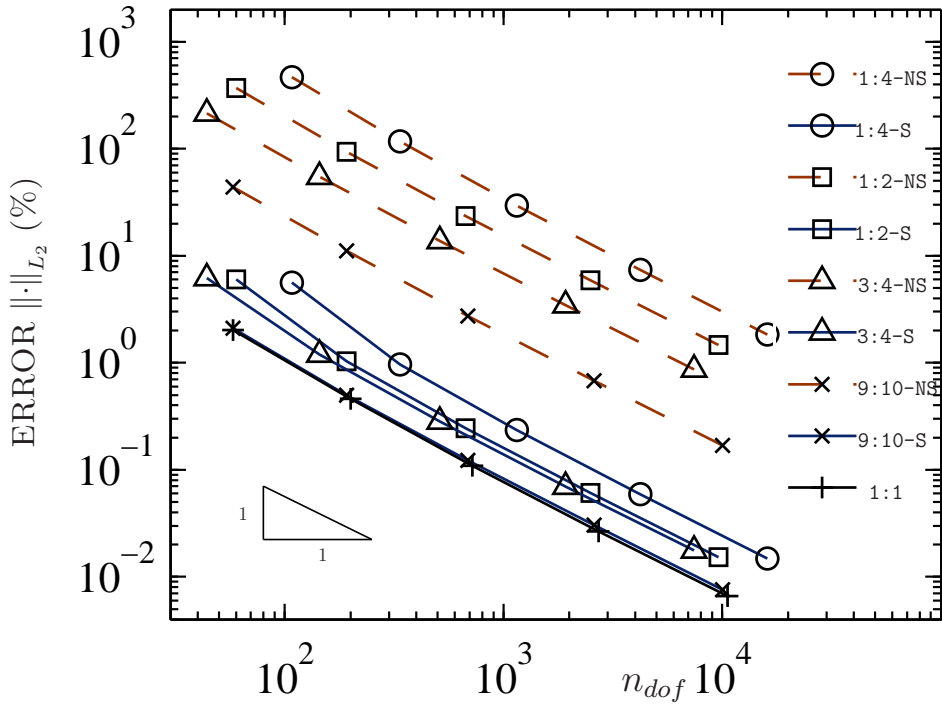
(b) Error in L_2 norm

Fig. 7. Error vs number of degrees of freedom.

15

tion. In the non smoothed method the convergence is the same. Therefore a constant gap between the error associated with both methods remains as the number of degrees of freedom is increased.

As pointed out above, another alternative to the smoothing technique would be the use of unsmoothed quadratic elements that should perform well in this kind of problems with curved surfaces.

5.2 Large deformation rings

The problem schematically shown in figure 8 was previously used in [15] to test the mortar method. It is a large deformation contact problem of two rings. Two material behaviour are considered for the rings: first elastic and then elastoplastic. In the first case the Young's modulus is $E = 689.56$ and the Poisson ratio $\upsilon = 0.32$. In the second case we add a plastic von Mises model with yield strength $S_y = 310$ and kinematic hardening with $H = 2.612$. The upper ring is being subject to a horizontal displacement with maximum value of $u_x = 28$ which is applied in 50 time increments.
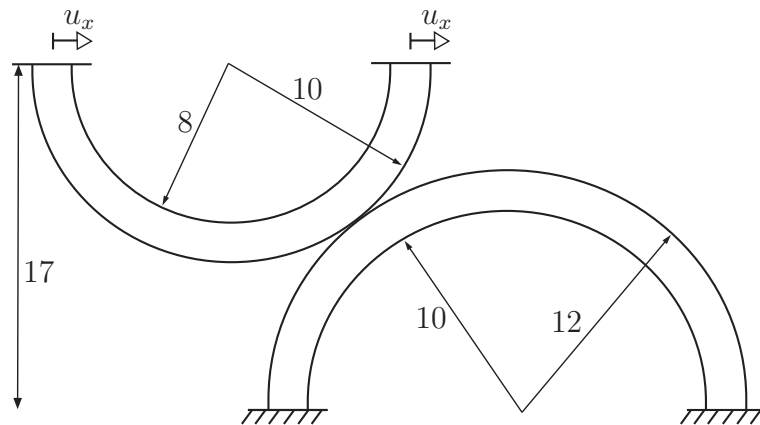

Fig. 8. Large deformation rings.

Figure 9 shows the deformed configuration and the von Mises stress field for elastic and plastic behavior and for different time steps. This problem was solved to test the convergence of the Newton iterations. This information is shown in table 1 for two time steps. As can be seen the convergence is good and the solution is obtained in 6 time steps. The simulation is quasistatic so in the case of the elastic behavior there is a snapthrough phenomenon during the simulation that affects the convergence.
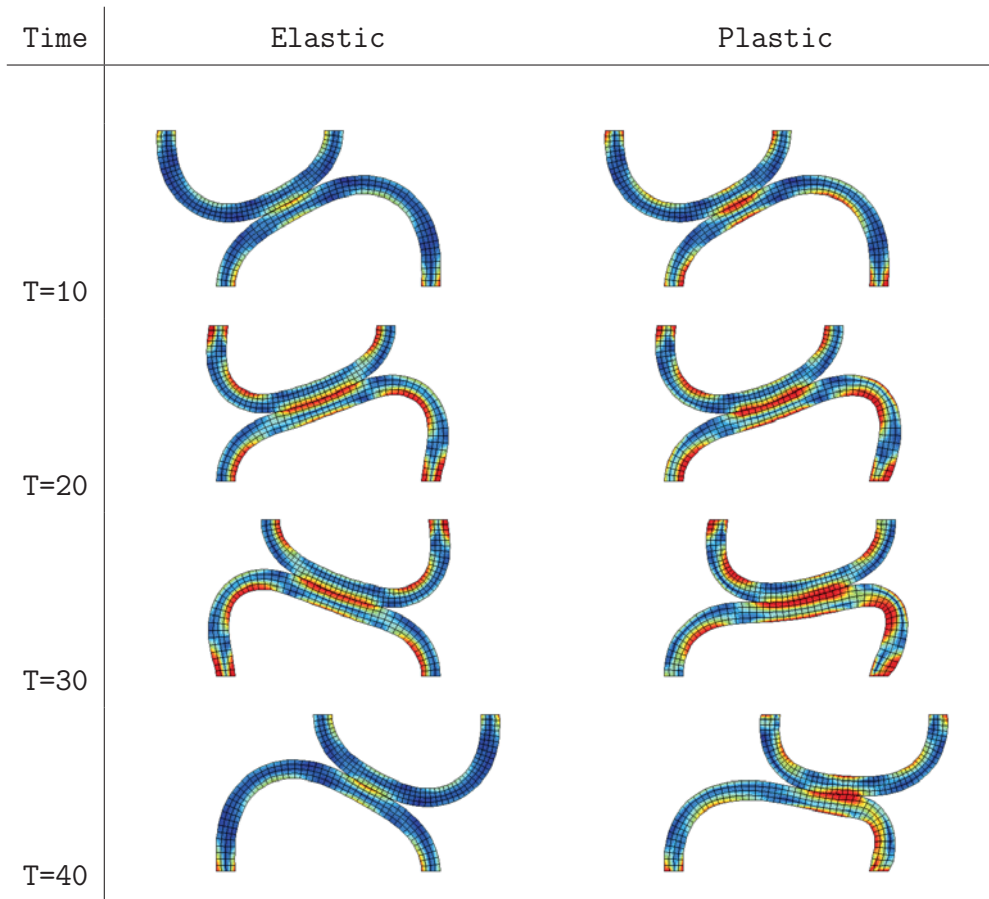
16

Time	Elastic	Plastic

Fig. 9. Von Mises stress field at different time steps.

Iteration	Elastic (T=10)	Plastic (T=10)	Elastic (T=30)	Plastic (T=30)
1	147.9	156.0	147.9	145.8
2	$2.61 \cdot 10^{-2}$	$3.13 \cdot 10^{-2}$	$3.45 \cdot 10^{-2}$	$2.96 \cdot 10^{-2}$
3	$8.38 \cdot 10^{-4}$	$1.15 \cdot 10^{-3}$	$1.19 \cdot 10^{-4}$	$9.85 \cdot 10^{-4}$
4	$1.08 \cdot 10^{-7}$	$3.63 \cdot 10^{-7}$	$6.85 \cdot 10^{-8}$	$1.75 \cdot 10^{-7}$
5	$1.45 \cdot 10^{-11}$	$6.82 \cdot 10^{-11}$	$4.00 \cdot 10^{-11}$	$3.78 \cdot 10^{-11}$
6	$2.12 \cdot 10^{-16}$	$1.58 \cdot 10^{-14}$	$3.83 \cdot 10^{-15}$	$7.76 \cdot 10^{-15}$

Table 1
 Convergence in energy norm.

5.3   Disc in contact semicircular hole

In this problem, also with large deformations, a solid disc interacts with a fixed base as depicted in figure 10. The radius of the disc and the contact surface of the base is $R = 50$ whilst the external radius of the base is $R_e = 125$. Neo-hookean material is assumed for both solids being the elastic constants

17

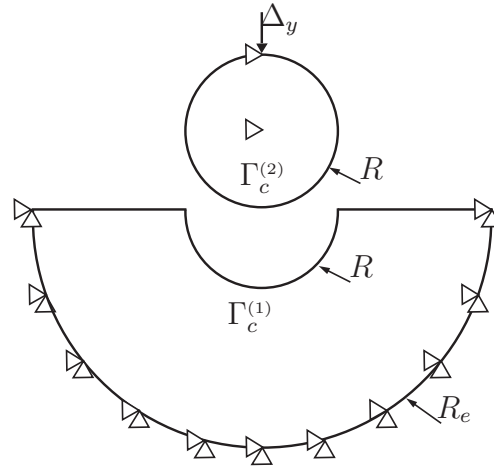of the disc $E_1 = 10^5$ and $\nu = 0.3$ and the base $E_2 = 10^3$ and $\nu = 0.3$.

Fig. 10. Schematic of the disc contact problem.

The solid disc is imposed to move in vertical direction with 20 time increments, for a maximum displacement $u_y = 90$. Figure 11 shows the deformed configuration for different time steps.

In figures 12 and 13 the contact pressure is shown for different time steps. We show results for the proposed smooth formulation and the non-sooth formulation in order to compare both methods. Theoretically, the two undeformed contact surfaces are equal and therefore the gap should be zero. But due to the different discretization of the two contacting bodies there is an error in the gap that affects to the contact pressure, mainly in the first time steps (T=1 and T=5). As can be seen in those initial time steps, the smooth formulation obtains a smoother distribution of the contact pressure because the error in the gap is smaller. Once the deformation becomes more important and higher values of the contact pressure are obtained, the error computing the gap has lower influence in the solution and a similar distribution of the contact pressure is obtained for both formulations.

5.4   Spur gears

The last example is the contact between two spur gears that undergo large rotations. The schematic of the problem is shown in figure 14. The two gears are equal and have a number of teeth $z = 22$, modulus $m = 10$ and width $b = 120$ mm. The power transmitted is $P = 70$ kW at a speed of $\omega = 11$ rad/s. The material is steel with elastic constants $E = 210$ GPa and $\nu = 0.3$, and is modelled using a St.Venant-Kirchhoff material model.

The boundary conditions are applied through the thick line shown in every body in figure 14. In the thick line the degrees of freedom are constrained to
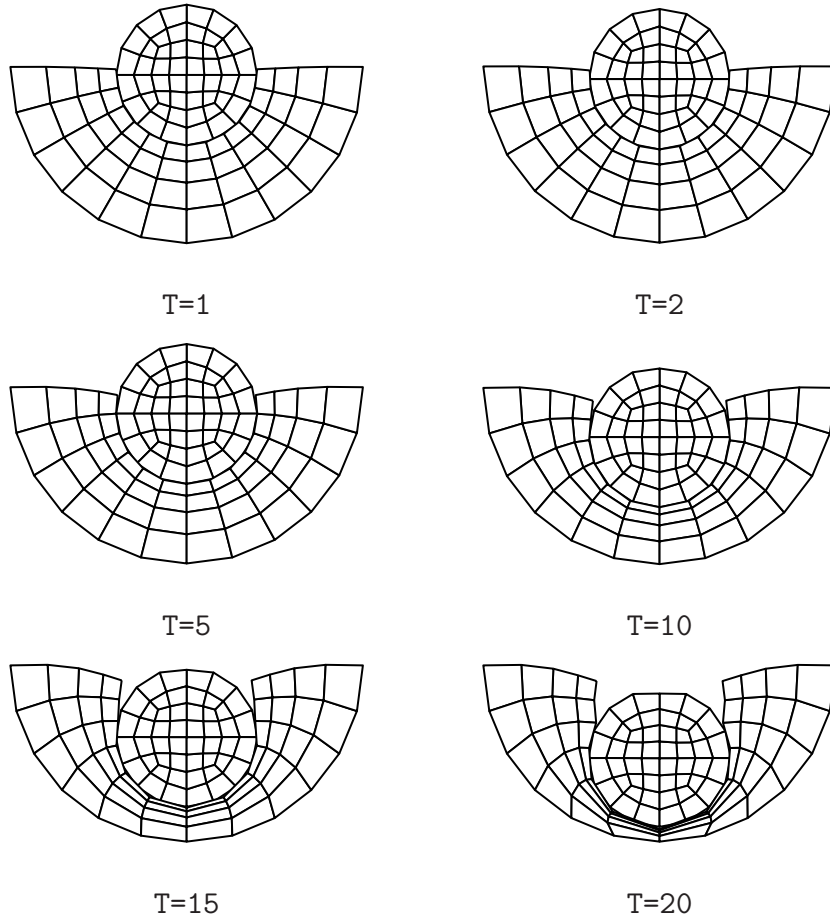
Fig. 11. Deformed configuration of the disc contact problem for different time steps.

have only a circular movement with respect to the gear center. In the upper gear a constant torque $T = 6366.2$ Nm is applied whilst the lower gear is imposed to move with different angles from $\theta = 0$ to $\theta = 2\pi/z$ in 100 time increments.

The contact ratio $\epsilon_\alpha = 1.6$ so the power is transmitted through two teeth during part of the time as can be seen in the position of figure 14 and through one tooth the rest of the time. To illustrate this, from the finite element results of contact pressure, the torque transmitted by each tooth can be computed. This was done by computing the resultant force in each contact area multiplied by the distance to the center of the gear. The results obtained are plotted in figure 15 where the blue line with the circle symbol is used for the torque transmitted by tooth 1, the red line with squared symbol for tooth 2 and the black line with star symbol for tooth 3. These torques are plotted for different time steps which are proportional to the the angle of rotation of the lower gear. In this figure there is a comparison of the results obtained with the non-smoothing and the smoothing formulations. As can be seen both formulations tend to yield similar results and there are oscillations on the torque transmitted
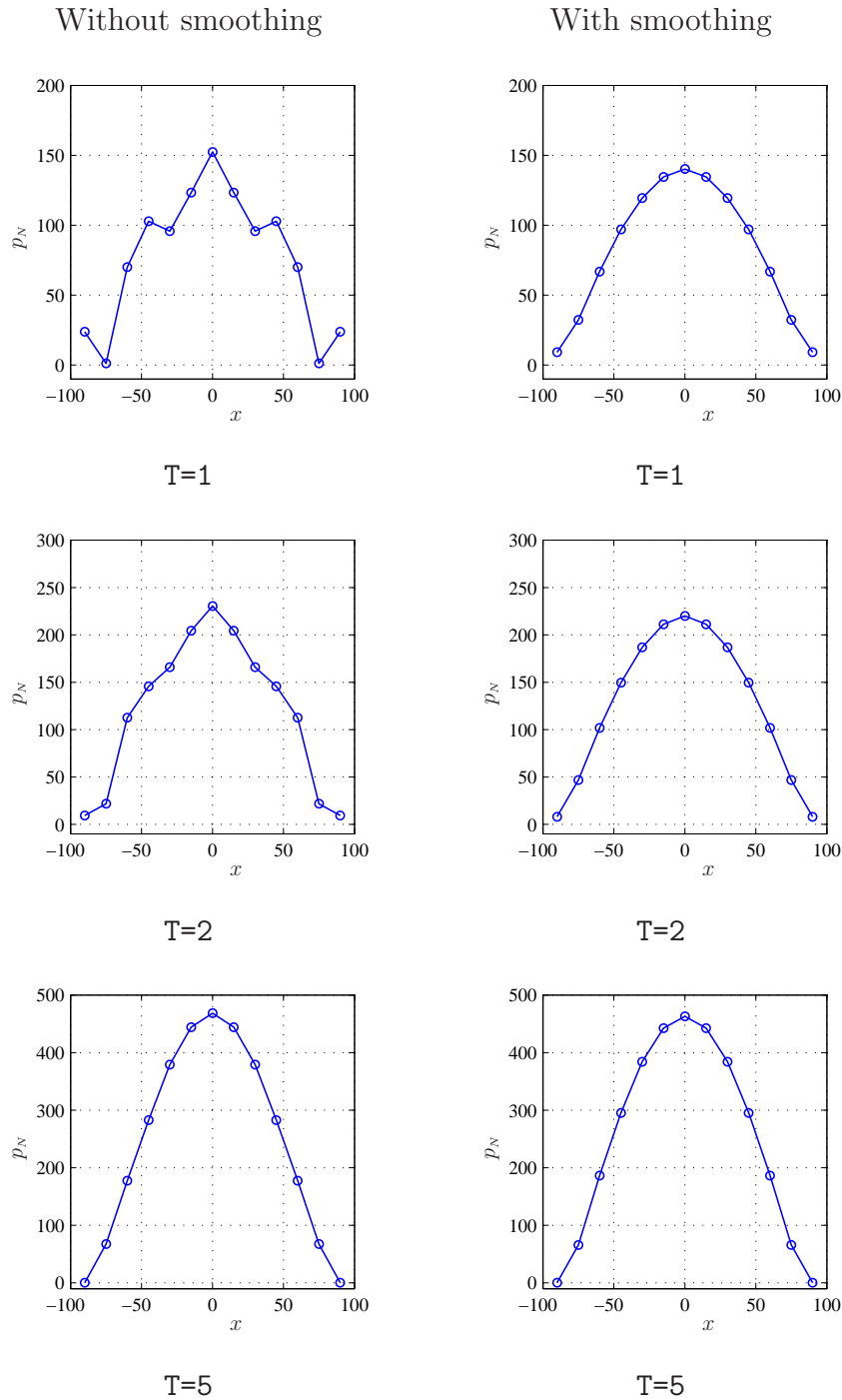
Fig. 12. Contact pressure distribution on the disc (time steps 1, 2 and 5).

by each tooth.

The oscillating results shown in figure 15 are due to the mesh which is too coarse for this problem. We have used an h-adaptive mesh refinement based on element subdivision [20] to obtain a mesh with a lower error. The mesh refinement introduces new nodes that adjust to the evolving profile of the teeth
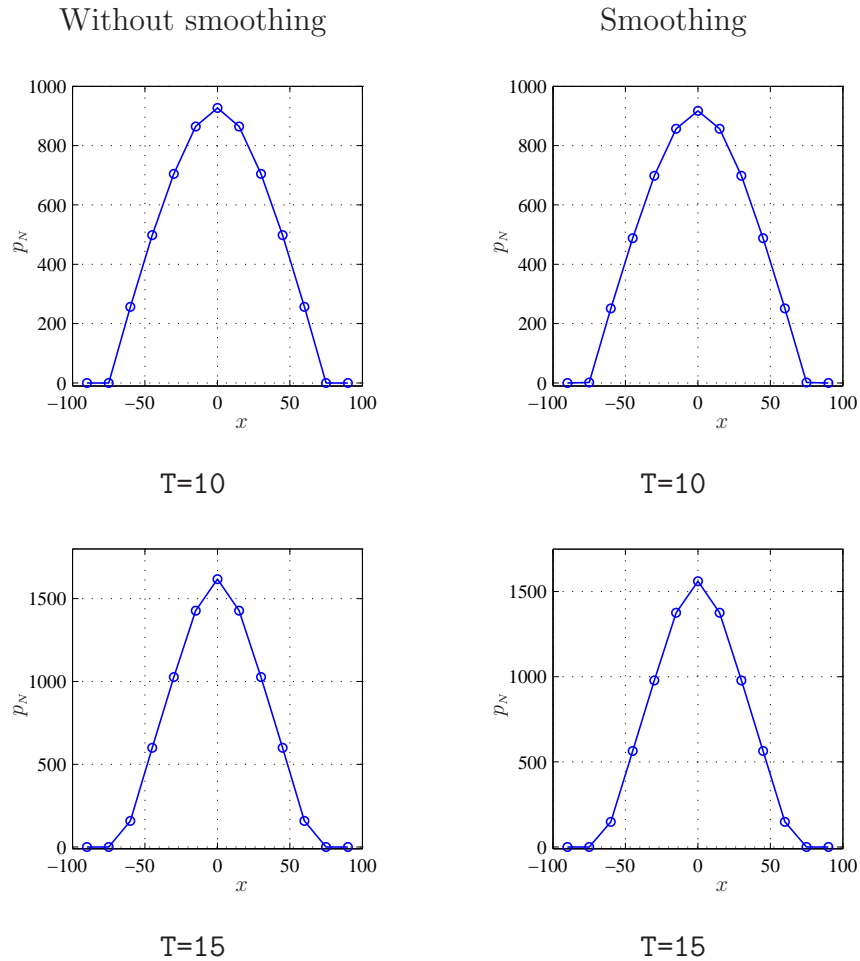
Fig. 13. Contact pressure distribution on the disc (time steps 10 and 15).

obtaining a more accurate representation of the real geometry. It adaptivity process uses information of the finite element error in all the time steps [21]. In figure 16 the last mesh of the sequence is shown and in figure 17 the torque transmitted by each tooth is plotted. Both smoothed and non-smoothed formulation are virtually the same. Again the blue line with circle symbol is used for the torque transmitted by tooth 1, the red line with square symbol for tooth 2 and the black line with star symbol for tooth 3. As can be seen the oscillations of the transmitted torque disappear.

One can distinguish several zones in the blue line with circle symbol. A first part with constant transmitted torque corresponds to the situation when there is only one tooth in contact. Two zones with high slope (between time $t = 3$ to $t = 9$ and between $t = 41$ to $t = 46$) result when another tooth is moving out of contact (first case) or is beginning to contact (second case). The high slope in the variation of the torque is due to the elastic deformation caused by the new contact force. Finally there is a second linear zone with lower slope that is due to the variation of the position of the contact point in the tooth
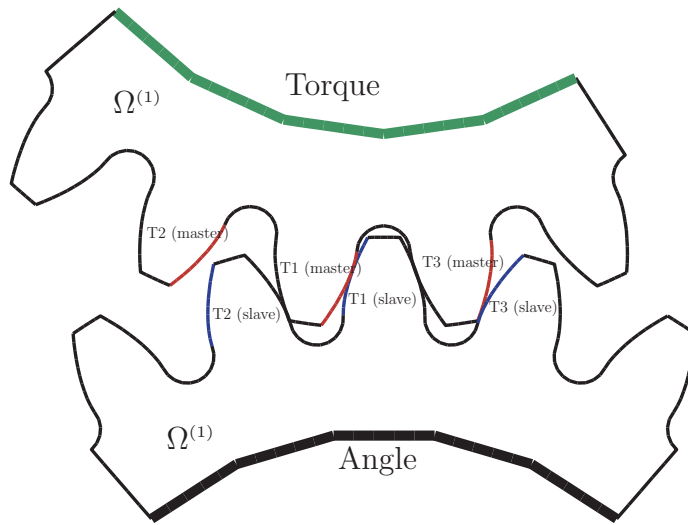
(a) Model
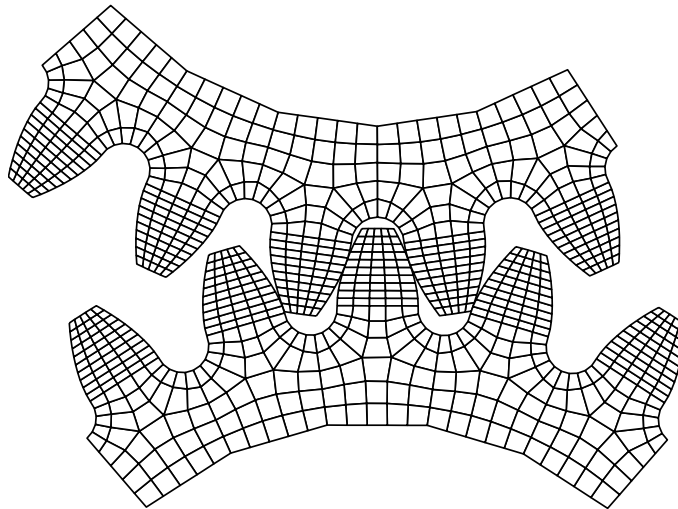
(b) Mesh

Fig. 14. Schematic of the straight gear contact problem.

profile, i.e. the resultant force is at a different distance from the gear center.

6   Conclusions

A smoothed segment-to-segment formulation has been presented to solve large deformation frictionless contact problems. The master and slave surfaces are defined using cubic Hermite polynomials on a first-order finite element mesh. The contact variables and integrals have been derived to solve the contact
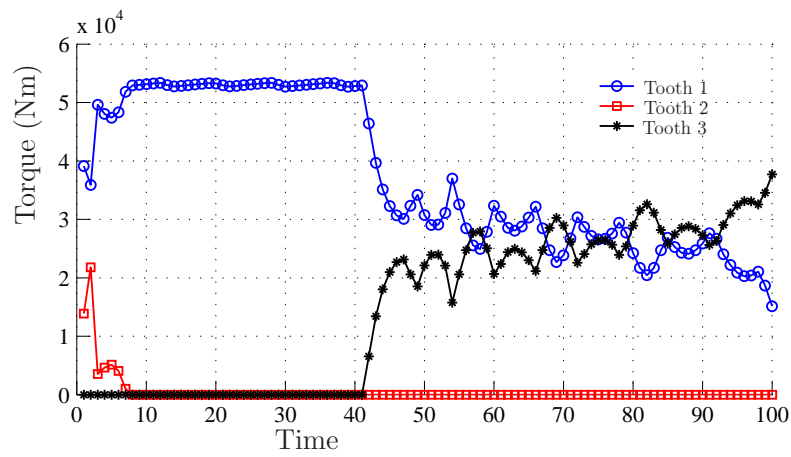
(a) Non-smoothing
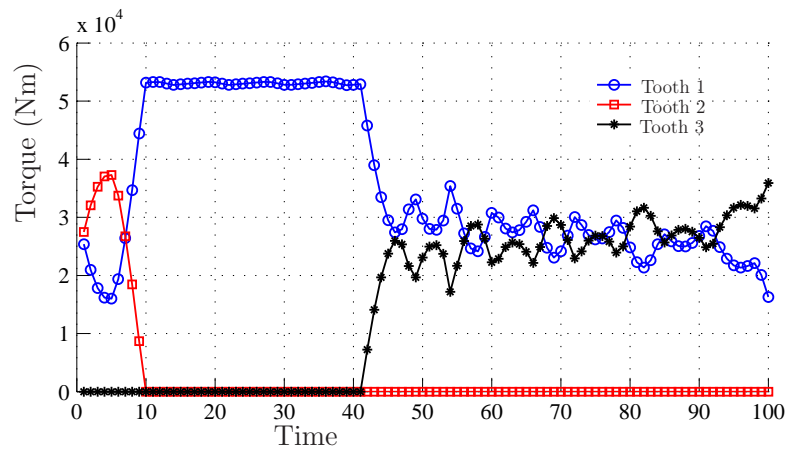
(b) Smoothing

Fig. 15. Torque transmitted by each tooth for the non-smoothing and smoothing formulations.

Fig. 16. 5th mesh obtained with the h-adaptative mesh refinement.

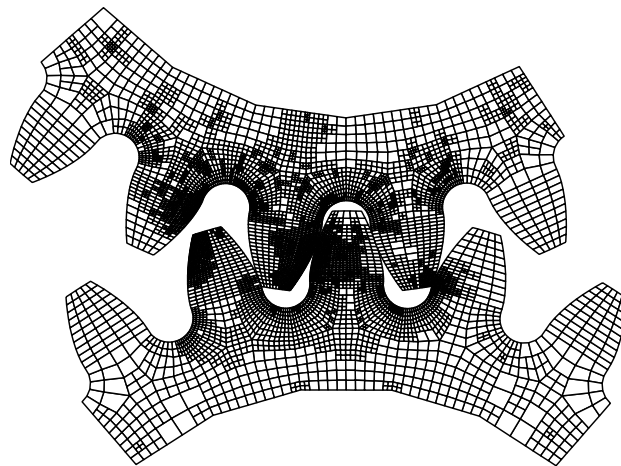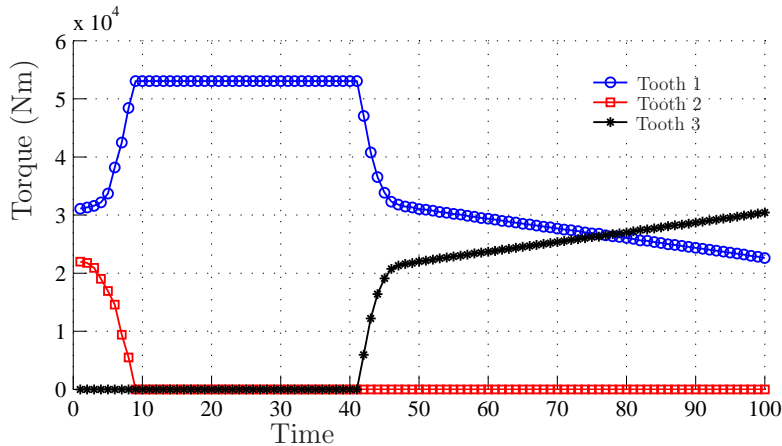Fig. 17. Torque transmitted by each tooth for the adapted mesh.

problem using the mortar method.

Numerical problems were solved to compare the proposed smoothed segment-to-segment formulation with the non-smoothed mortar formulation presented in [13]. The results show an improvement in the solution in the case of smoothed formulation for problems with matching curved surfaces discretized using non-conforming meshes. In those cases, the global finite element error is affected by the error in computing the initial gap in addition to the discretization error. The initial gap computed using the cubic polynomial of the smoothed formulation is more accurate than that computed using the linear surface of the non-smoothed formulation, improving the finite element solution. The use of quadratic elements could also reduce the error due to initial gap.

In some examples, like the contact problem between two spur gears, the results obtained with the smoothing and non-smoothing formulation are very similar and improvement of the finite element solution has been obtained using an h-adaptive mesh refinement that adjust the new nodes to the evolving profile of the teeth.

In previous works and for frictional problems the smoothing technique has been applied to node-to-segment formulation to reduce oscillations in the forces transmitted for sliding meshes and to obtain more robust algorithms. However, the non-smoothed mortar formulation already overcomes this type of oscillations that appear in frictional problems. Therefore, the type of improvement that can be achieved with smoothed mortar formulation is not essentially related to the frictional character of the problem but with the existence of non matching meshes on curved surfaces.

24

A   Appendix

A.1   Linearization of unit vectors and the jacobian

The variation and linearization of the unit tangent vector (or the unit normal vector) is obtained taking into account the definition of equation 17 as

$$\delta \mathbf{s}_g^{(1)} = \frac{\delta \hat{\mathbf{s}}_g^{(1)}}{\|\hat{\mathbf{s}}_g^{(1)}\|} - \frac{\left(\hat{\mathbf{s}}_g^{(1)} \cdot \delta \hat{\mathbf{s}}_g^{(1)}\right) \hat{\mathbf{s}}_g^{(1)}}{\|\hat{\mathbf{s}}_g^{(1)}\|^3} \tag{A.1}$$

And linearization of the variation

$$\Delta \delta \mathbf{s}_g^{(1)} = 3 \frac{\hat{\mathbf{s}}_g^{(1)} \left(\Delta \hat{\mathbf{s}}_g^{(1)} \cdot \hat{\mathbf{s}}_g^{(1)}\right) \left(\delta \hat{\mathbf{s}}_g^{(1)} \cdot \hat{\mathbf{s}}_g^{(1)}\right)}{\|\hat{\mathbf{s}}_g^{(1)}\|^3} - \frac{\hat{\mathbf{s}}_g^{(1)} \left(\Delta \hat{\mathbf{s}}_g^{(1)} \cdot \delta \hat{\mathbf{s}}_g^{(1)}\right)}{\|\hat{\mathbf{s}}_g^{(1)}\|^3}$$
$$- \frac{\delta \hat{\mathbf{s}}_g^{(1)} \left(\Delta \hat{\mathbf{s}}_g^{(1)} \cdot \hat{\mathbf{s}}_g^{(1)}\right)}{\|\hat{\mathbf{s}}_g^{(1)}\|^3} - \frac{\Delta \hat{\mathbf{s}}_g^{(1)} \left(\delta \hat{\mathbf{s}}_g^{(1)} \cdot \hat{\mathbf{s}}_g^{(1)}\right)}{\|\hat{\mathbf{s}}_g^{(1)}\|^3} \tag{A.2}$$

The Jacobian of the coordinate transformation between the slave segment and the reference element is defined as

$$J_g = \frac{l^{(1)}}{2} = \frac{\sqrt{\left(\mathbf{x}_{ks}^{(1)} - \mathbf{x}_{ks-1}^{(1)}\right) \cdot \left(\mathbf{x}_{ks}^{(1)} - \mathbf{x}_{ks-1}^{(1)}\right)}}{2} \tag{A.3}$$

The linearization and variation can be written as

$$\delta J_g = -\frac{1}{2} \mathbf{s}_{c_{ks}}^{(1)} \cdot \left(\mathbf{v}_{ks}^{(1)} - \mathbf{v}_{ks-1}^{(1)}\right) \tag{A.4}$$

$$\Delta \delta J_g = \frac{1}{2\, l^{(1)}} \left(\mathbf{v}_{ks}^{(1)} - \mathbf{v}_{ks-1}^{(1)}\right) \cdot \left(\Delta \mathbf{x}_{ks}^{(1)} - \Delta \mathbf{x}_{ks-1}^{(1)}\right)$$
$$- \frac{1}{2\, l^{(1)}} \mathbf{s}_{c_{ks}}^{(1)} \cdot \left(\mathbf{v}_{ks}^{(1)} - \mathbf{v}_{ks-1}^{(1)}\right) \mathbf{s}_{c_{ks}}^{(1)} \cdot \left(\Delta \mathbf{x}_{ks}^{(1)} - \Delta \mathbf{x}_{ks-1}^{(1)}\right) \tag{A.5}$$

Note that the tangent vector $\mathbf{s}_{c_{ks}}^{(1)}$ is constant for a segment and it is different from tangent vector $\hat{\mathbf{s}}^{(1)}$ which is derived from the smoothing surface definition.

B   Matrix notation

A patch of nodes ($ks - 2$, $ks-1$, ks, $ks+1$, $km - 2$, $km - 1$, km and $km+1$) can be defined associated to a quadrature point of every slave segment, as in the segment c_{ks} of figure 3. This patch can be used to express the contribution of the quadrature point to the tangent matrix of equation 29. The degrees of

freedom related to nodes in the patch are used to define the following vectors

$$\Delta\check{\mathbf{u}}^T = \left(\Delta\mathbf{u}^{(1)}_{ks-2}, \Delta\mathbf{u}^{(1)}_{ks-1}, \Delta\mathbf{u}^{(1)}_{ks}, \Delta\mathbf{u}^{(1)}_{ks+1}, \Delta\mathbf{u}^{(2)}_{km-2}, \Delta\mathbf{u}^{(2)}_{km-1}, \Delta\mathbf{u}^{(2)}_{km}, \Delta\mathbf{u}^{(2)}_{km+1}\right)$$
(B.1)

$$\delta\check{\mathbf{u}}^T = \left(\mathbf{v}^{(1)}_{ks-2}, \mathbf{v}^{(1)}_{ks-1}, \mathbf{v}^{(1)}_{ks}, \mathbf{v}^{(1)}_{ks+1}, \mathbf{v}^{(2)}_{km-2}, \mathbf{v}^{(2)}_{km-1}, \mathbf{v}^{(2)}_{km}, \mathbf{v}^{(2)}_{km+1}\right)$$
(B.2)

We define the following vectors and matrix that arise from linearization of the normal gap, normal vector and Jacobian determinant

$$
\begin{aligned}
\mathbf{F_n} = \Big[&-H^{(1)}_1 n^{(1)}_1 \ -H^{(1)}_1 n^{(1)}_2 \ -H^{(1)}_2 n^{(1)}_1 \ -H^{(1)}_2 n^{(1)}_2 \ -H^{(1)}_3 n^{(1)}_1 \ -H^{(1)}_3 n^{(1)}_2 \ \ldots \\
&\ldots \quad -H^{(1)}_4 n^{(1)}_1 \ -H^{(1)}_4 n^{(1)}_2 \ \ H^{(2)}_1 n^{(1)}_1 \ \ \ H^{(2)}_1 n^{(1)}_2 \quad \ldots \\
&\ldots \quad \ H^{(2)}_2 n^{(1)}_1 \ \ \ H^{(2)}_2 n^{(1)}_2 \ \ \ H^{(2)}_3 n^{(1)}_1 \ \ \ H^{(2)}_3 n^{(1)}_2 \quad \ldots \\
&\ldots \quad \ H^{(2)}_4 n^{(1)}_1 \ \ \ H^{(2)}_4 n^{(1)}_2 \Big]^T
\end{aligned}
$$
(B.3)

$$
\begin{aligned}
\mathbf{F_s} = \Big[&-H^{(1)}_1 s^{(1)}_1 \ -H^{(1)}_1 s^{(1)}_2 \ -H^{(1)}_2 s^{(1)}_1 \ -H^{(1)}_2 s^{(1)}_2 \ -H^{(1)}_3 s^{(1)}_1 \ -H^{(1)}_3 s^{(1)}_2 \ \ldots \\
&\ldots \quad -H^{(1)}_4 s^{(1)}_1 \ -H^{(1)}_4 s^{(1)}_2 \ \ H^{(2)}_1 s^{(1)}_1 \ \ \ H^{(2)}_1 s^{(1)}_2 \quad \ldots \\
&\ldots \quad \ H^{(2)}_2 s^{(1)}_1 \ \ \ H^{(2)}_2 s^{(1)}_2 \ \ \ H^{(2)}_3 s^{(1)}_1 \ \ \ H^{(2)}_3 s^{(1)}_2 \quad \ldots \\
&\ldots \quad \ H^{(2)}_4 s^{(1)}_1 \ \ \ H^{(2)}_4 s^{(1)}_2 \Big]^T
\end{aligned}
$$
(B.4)

$$
\begin{aligned}
\mathbf{N_n} = \frac{1}{\|\hat{\mathbf{n}}^{(1)}_g\|} \Big[&-H^{(1)}_{1,\xi} n^{(1)}_2 \ \ H^{(1)}_{1,\xi} n^{(1)}_1 \ -H^{(1)}_{2,\xi} n^{(1)}_2 \ \ H^{(1)}_{2,\xi} n^{(1)}_1 \ \ldots \\
&\ldots \quad -H^{(1)}_{3,\xi} n^{(1)}_2 \ \ H^{(1)}_{3,\xi} n^{(1)}_1 \ -H^{(1)}_{4,\xi} n^{(1)}_2 \ \ H^{(1)}_{4,\xi} n^{(1)}_1 \ \ldots \\
&\ldots \qquad \quad 0 \qquad \quad 0 \qquad \quad 0 \qquad \quad 0 \qquad \ldots \\
&\ldots \qquad \quad 0 \qquad \quad 0 \qquad \quad 0 \qquad \quad 0 \Big]^T
\end{aligned}
$$
(B.5)

$$
\begin{aligned}
\mathbf{N_s} = \frac{1}{\|\hat{\mathbf{n}}^{(1)}_g\|} \Big[&-H^{(1)}_{1,\xi} s^{(1)}_2 \ \ H^{(1)}_{1,\xi} s^{(1)}_1 \ -H^{(1)}_{2,\xi} s^{(1)}_2 \ \ H^{(1)}_{2,\xi} s^{(1)}_1 \ \ldots \\
&\ldots \quad -H^{(1)}_{3,\xi} s^{(1)}_2 \ \ H^{(1)}_{3,\xi} s^{(1)}_1 \ -H^{(1)}_{4,\xi} s^{(1)}_2 \ \ H^{(1)}_{4,\xi} s^{(1)}_1 \ \ldots \\
&\ldots \qquad \quad 0 \qquad \quad 0 \qquad \quad 0 \qquad \quad 0 \qquad \ldots \\
&\ldots \qquad \quad 0 \qquad \quad 0 \qquad \quad 0 \qquad \quad 0 \Big]^T
\end{aligned}
$$
(B.6)

$$\mathbf{L_n} = [0 \ 0 \ -n^{(1)}_{c\,1} \ -n^{(1)}_{c\,2} \ n^{(1)}_{c\,1} \ n^{(1)}_{c\,2} \ 0 \ 0 \ 0 \ 0 \ 0 \ 0 \ 0 \ 0 \ 0 \ 0]^T$$
(B.7)

$$\mathbf{L_s} = [0 \ 0 \ -s^{(1)}_{c\,1} \ -s^{(1)}_{c\,2} \ s^{(1)}_{c\,1} \ s^{(1)}_{c\,2} \ 0 \ 0 \ 0 \ 0 \ 0 \ 0 \ 0 \ 0 \ 0 \ 0]^T$$
(B.8)

$$\mathbf{L} = \begin{bmatrix} 0 & 0 & -1 & 0 & 1 & 0 & 0 & 0 & 0 & 0 & 0 & 0 & 0 & 0 & 0 & 0 \\ 0 & 0 & 0 & -1 & 0 & 1 & 0 & 0 & 0 & 0 & 0 & 0 & 0 & 0 & 0 & 0 \end{bmatrix}^T$$
(B.9)

where $\mathbf{n}^{(1)} = \mathbf{n}^{(1)}_g$ and $\mathbf{s}^{(1)} = \mathbf{s}^{(1)}_g$ are the normal and tangent vectors computed from the smoothed surface definition, $\mathbf{n}^{(1)}_c = \mathbf{n}^{(1)}_{c_{ks}}$ is the normal vector to the

slave segment, $\mathbf{s}_c^{(1)} = \mathbf{s}_{c_{ks}}^{(1)}$ is the tangent vector defining the slave segment and $H_{i,\xi}$ is the derivative of the Hermite interpolation function defined in equation 16, with respect to the local coordinate.

We also define the following values

$$p_{sm} = \hat{\mathbf{s}}^{(2)} \cdot \mathbf{n}_g^{(1)} \qquad l_{sm} = \hat{\mathbf{s}}^{(2)} \cdot \mathbf{s}_g^{(1)} \tag{B.10}$$

With these definitions and assuming that the node ks is active, the contribution of a quadrature point to the contact force vector (equation 10) can be expressed in matrix form as

$$\mathbf{f}_N^c = H_g \, J_g \, M_{ks}^{(1)} \, \lambda_{Nks} \left(\mathbf{F_n} - \frac{p_{sm}}{l_{sm}} \mathbf{F_s} + \frac{p_{sm} \, g_{Ng}}{l_{sm}} \mathbf{N_s} \right) \tag{B.11}$$

The tangent matrix is obtained from equations 25. We first need to define the following matrices (from equations 22 and 23)

$$
\begin{aligned}
\mathbf{M_t} =& \frac{1}{2 \, l_{sm}^2} \left(\mathbf{F_s} \otimes \mathbf{L_s} + \mathbf{L_s} \otimes \mathbf{F_s} \right) - \frac{g_{Ng}}{2 \, l_{sm}^2} \left(\mathbf{N_s} \otimes \mathbf{L_s} + \mathbf{L_s} \otimes \mathbf{N_s} \right) \\
&+ \frac{1}{l_{sm}} \left(\mathbf{F_n} \otimes \mathbf{N_s} + \mathbf{N_s} \otimes \mathbf{F_n} \right) - \frac{p_{sm}}{l_{sm}^2} \left(\mathbf{F_s} \otimes \mathbf{N_s} + \mathbf{N_s} \otimes \mathbf{F_s} \right) \\
&+ \frac{2 \, p_{sm} \, g_{Ng}}{l_{sm}^2} \mathbf{N_s} \otimes \mathbf{N_s} - \frac{g_{Ng}}{l_{sm}} \left(\mathbf{N_n} \otimes \mathbf{N_s} + \mathbf{N_s} \otimes \mathbf{N_n} \right)
\end{aligned}
\tag{B.12}
$$

$$
\begin{aligned}
\mathbf{M_n} =& -\frac{1}{2 \, l_{sm}} \left(\mathbf{F_s} \otimes \mathbf{L_n} + \mathbf{L_n} \otimes \mathbf{F_s} \right) + \frac{g_{Ng}}{2 \, l_{sm}} \left(\mathbf{N_s} \otimes \mathbf{L_n} + \mathbf{L_n} \otimes \mathbf{N_s} \right) \\
&+ p_{sm} \, \mathbf{M_t} - g_{Ng} \, \mathbf{N_n} \otimes \mathbf{N_n} + \frac{g_{Ng}}{l^{(1)2}} \mathbf{N}^T \mathbf{N}
\end{aligned}
\tag{B.13}
$$

From equation 25, taking the integrals 2, 3, 5 and 6, we obtain

$$
\begin{aligned}
\mathbf{K_N} =& H_g \, M_{ks}^{(1)} \, \lambda_{Nks} \left[\mathbf{M_n} \, J_g - \frac{1}{2} \left(\mathbf{L_s} \otimes \mathbf{F_n} + \mathbf{F_n} \otimes \mathbf{L_s} \right) \right) \\
&+ \frac{p_{sm}}{2 \, l_{sm}} \left(\mathbf{L_s} \otimes \mathbf{F_s} + \mathbf{F_s} \otimes \mathbf{L_s} \right) - \frac{p_{sm} \, g_{Ng}}{2 \, l_{sm}} \left(\mathbf{L_s} \otimes \mathbf{N_s} + \mathbf{N_s} \otimes \mathbf{L_s} \right) \\
&+ \frac{g_{Ng}}{2 \, l^{(1)}} \mathbf{L}^T \mathbf{L} - \frac{g_{Ng}}{2 \, l^{(1)}} \mathbf{L_s} \otimes \mathbf{L_s} \Bigg]
\end{aligned}
\tag{B.14}
$$

Taking integrals 1 and 4 from equation 25 the contact constraint coefficient matrix is obtained

$$\mathbf{C}_N^T = H_g \, M_{ks}^{(1)} \left[J_g \left(\mathbf{F_n} - \frac{p_{sm}}{l_{sm}} \mathbf{F_s} + \frac{p_{sm} \, g_{Ng}}{l_{sm}} \mathbf{N_s} \right) - \frac{g_{Ng}}{2} \mathbf{L_s} \right] \tag{B.15}$$

Acknowledgement

References

[1] M.A. Puso and T. Laursen. A mortar segment-to-segment contact method for large deformation solid mechanics. *Computer Methods in Applied Mechanics and Engineering*, 193:601–629, 2004.

[2] M.A. Puso and T. Laursen. A mortar segment-to-segment frictional contact method for large deformations. *Computer Methods in Applied Mechanics and Engineering*, 193:4891–4913, 2004.

[3] B. Yang, T. Laursen, and X. Meng. Two dimensional mortar contact methods for large deformation frictional sliding. *International Journal for Numerical Methods in Engineering*, 62:1183–1225, 2005.

[4] K.A. Fischer and P. Wriggers. Frictionless 2D contact formulations for finite deformations based on the mortar method. *Computational Mechanics*, 36:226–244, 2005.

[5] K.A. Fischer and P. Wriggers. Mortar based frictional contact formulation for higher order interpolations using the moving friction cone. *Computer Methods in Applied Mechanics and Engineering*, 195:5020–5036, 2006.

[6] S. Hueber, A. Matei, and B. I. Wohlmuth. Efficient algorithms for problems with friction. *SIAM Journal on Scientific Computing*, 29(1):70–92, 2007.

[7] M.A. Puso, T.A. Laursen, and J. Solberg. A segment-to-segment mortar contact method for quadratic elements and large deformations. *Computer Methods in Applied Mechanics and Engineering*, 197:555–566, 2008.

[8] S. Hartmann and E. Ramm. A mortar based contact formulation for non-linear dynamics using dual lagrange multipliers. *Finite Elements in Analysis and Design*, 44:245–258, 2008.

[9] A. Popp, M.W. Gee, and W.A. Wall. A finite deformation mortar contact formulation using a primal-dual active set strategy. *International Journal for Numerical Methods in Engineering*, 79:1354–1391, 2009.

[10] A. Popp, M. Gitterle, M.W. Gee, and W.A. Wall. A dual mortar approach for 3D finite deformation contact with consistent linearization. *International Journal for Numerical Methods in Engineering*, 83:1428–1465, 2010.

[11] M. Gitterle, A. Popp, M.W. Gee, and W.A. Wall. Finite deformation frictional mortar contact using a semi-smooth newton method with consistent

linearization. *International Journal for Numerical Methods in Engineering*, 84:543–571, 2010.

[12] C. Hesch and P. Betsch. A mortar method for energy-momentum conserving schemes in frictionless dynamic contact problems. *International Journal for Numerical Methods in Engineering*, 77:1468–1500, 2009.

[13] M. Tur, J. Fuenmayor, and P. Wriggers. A mortar-based frictional contact formulation for large deformations using lagrange multipliers. *Computer Methods in Applied Mechanics and Engineering*, 198:2860–2873, 2009.

[14] P. Wriggers, L. Krstulovic-Opara, and J. Korelc. Smooth C^1-interpolations for two-dimensional frictional contact problems. *International Journal for Numerical Methods in Engineering*, 51:1469–1495, 2001.

[15] V. Padmanabhan and T.A. Laursen. A framework for development of surface smoothing procedures in large deformation frictional contact analysis. *Finite Elements in Analysis and Design*, 37:173–198, 2001.

[16] M. Al-Dojayli and S.A. Meguid. Accurate modeling of contact using cubic splines. *Finite Elements in Analysis and Design*, 38:337–352, 2002.

[17] M.A. Puso and T.A. Laursen. A 3D contact smoothing method using gregory patches. *International Journal for Numerical Methods in Engineering*, 54:11611194, 2002.

[18] L. Krstulovic. *C^1-continuous formulation for finite deformation contact.* PhD thesis, Universitat Hannover, 2001.

[19] D. Chamoret, P. Saillard, A. Rassineux, and J.M. Bergheau. New smoothing procedures in contact mechanics. *Journal of Computational and Applied Mathematics*, 168:107–116, 2004.

[20] M. Tur, F.J. Fuenmayor, J.J. Rodenas, and E. Giner. 3D analysis of the influence of specimen dimensions on fretting stresses. *Finite Elements in Analysis and Design*, 39 (10):933–949, 2003.

[21] M. Tur. *Modelado de problemas de contacto mediante elementos finitos utilizando tcnicas de interaccin segmento-segmento.* PhD thesis, Universitat Politecnica de Valencia, 2008.